Bull Volcanol (2011) 73:73–90
DOI 10.1007/s00445-010-0404-5

RESEARCH ARTICLE

A quantitative uncertainty assessment of eruptive parameters derived from tephra deposits: the example of two large eruptions of Cotopaxi volcano, Ecuador

Sébastien Biass · Costanza Bonadonna

Received: 20 October 2009 / Accepted: 26 August 2010 / Published online: 19 September 2010

Abstract Physical parameters of explosive eruptions are typically derived from tephra deposits. However, the characterization of a given eruption relies strongly on the quality of the dataset used, the strategy chosen to obtain and process field data and the particular model considered to derive eruptive parameters. As a result, eruptive parameters are typically affected by a certain level of uncertainty and should not be considered as absolute values. Unfortunately, such uncertainty is difficult to assess because it depends on several factors and propagates from field sampling to the application and interpretation of dispersal models. Characterization of explosive eruptions is made even more difficult when tephra deposits are poorly exposed and only medial data are available. In this paper, we present a quantitative assessment of the uncertainty associated with the characterization of tephra deposits generated by the two largest eruptions of the last 2,000 years of Cotopaxi volcano, Ecuador. In particular, we have investigated the effects of the determination of the maximum clast on the compilation of isopleth maps, and, therefore, on the characterization of plume height. We have also compared the results obtained from the application of different models for the determination of both plume height and erupted volume and for the eruption classification. Finally, we have investigated the uncertainty propagation into the calculation of mass eruption rate and eruption duration. We have found that for our case study, the determination of plume height from isopleth maps is more sensitive to the averaging techniques used to define the maximum clast than to the choice of dispersal models used (i.e. models of Carey and Sparks 1986; Pyle 1989) and that even the application of the same dispersal model can result in plume height discrepancies if different isopleth lines are used (i.e. model of Carey and Sparks 1986). However, the uncertainties associated with the determination of erupted mass, and, as a result, of the eruption duration, are larger than the uncertainties associated with the determination of plume height. Mass eruption rate is also associated with larger uncertainties than the determination of plume height because it is related to the fourth power of plume height. Eruption classification is also affected by data processing. In particular, uncertainties associated with the compilation of isopleth maps affect the eruption classification proposed by Pyle (1989), whereas the VEI classification is affected by the uncertainties resulting from the determination of erupted mass. Finally, we have found that analytical and empirical models should be used together for a more reliable characterization of explosive eruptions. In fact, explosive eruptions would be characterized better by a range of parameters instead of absolute values for erupted mass, plume height, mass eruption rate and eruption duration. A standardization of field sampling would also reduce the uncertainties associated with eruption characterization.

Keywords Tephra · Eruptive parameters · Volume · Plume height · Mass eruption rate · Maximum clast · Cotopaxi

Editorial responsibility: P. Delmelle

S. Biass (✉) · C. Bonadonna
Département de Minéralogie, Université de Genève,
Rue des Maraîchers 13,
CH-1205 Geneva, Switzerland
e-mail: biasse3@etu.unige.ch

Introduction

Tephra deposits are an important source of information necessary to constrain physical parameters of explosive eruptions. In particular, the distribution of deposit thickness

around the vent, which is commonly presented in the form of isopach maps, can be used to derive the erupted volume (e.g. Pyle 1989, 1995; Legros 2000; Fierstein and Nathenson 1992; Bonadonna and Houghton 2005; Sulpizio 2005), whereas the distribution of the largest clasts, commonly presented in the form of isopleth maps, can be used to derive the maximum plume height and maximum wind speed at the time of the eruption (e.g. Carey and Sparks 1986; Pyle 1989). Mass eruption rate (MER) and eruption duration can be derived from different combinations of the associated results on erupted volume and column height (e.g. Wilson and Walker 1987; Sparks 1986).

However, constraining physical parameters of a given eruption is not straightforward and relies strongly on (a) the quality of available data, which is a direct reflection of the deposit exposure, (b) the strategy chosen to process field data, e.g. data interpretation and averaging, and (c) the particular model and combination of models used to derive eruptive parameters. As a result, eruptive parameters derived from the application of dispersal models are affected by a certain level of uncertainty and should not be considered as absolute values. Unfortunately, the level of such uncertainty is difficult to assess because it depends on several factors and propagates from field sampling to the application and interpretation of both empirical and analytical models. In this paper, we present a quantitative assessment of the uncertainty associated with the characterization of two tephra deposits generated by Cotopaxi volcano, Ecuador: layers 3 and 5 described in Barberi et al. (1995). The objective of this paper is not model validation but a thorough analysis of uncertainty propagation from field sampling through the calculation of plume height, erupted mass, mass eruption rate and eruption duration in the case of past eruptions where tephra deposits are only partially preserved.

Cotopaxi is a young stratovolcano situated in the middle portion of the Interandean Depression in the Cordilleras of Ecuador. The stratigraphic record of the past 2,000 years contains 22 tephra layers of basaltic-andesitic to andesitic composition, mainly generated by sustained explosive eruptions of high dispersive power, high intensity, but moderate magnitudes (Barberi et al. 1995; Hall and Mothes 2008). Layer 3 is the most voluminous pumice fallout bed of the last 2000-year activity at Cotopaxi, with an age of 820± 80 years B.P. (Barberi et al. 1995). It also represents the most silicic event of the last 5,000 years (whole-rock composition of 62 wt% SiO_2; Barberi et al. 1995). Although some smaller subunits can be defined, the main dominant Plinian deposit is a well-sorted pumice bed, bearing sub-centimetric lithic fragments of andesitic lavas. Layer 5 is a black scoriaceous lapilli fallout with an age of 1,180±80 years B.P. (Barberi et al. 1995). This bed, with clasts having a whole-rock silica content of 58 wt.% is characterised by an abundance of grey lava lithics (Barberi et al. 1995).

In order to quantify the uncertainty associated with the characterization of layers 3 and 5 of Cotopaxi volcano, we have assessed the influence of different clast-averaging techniques for the compilation of isopleth maps on the estimation of column height, MER, duration and eruption style. We have also assessed the discrepancies resulting from the application of different empirical and analytical models for the calculation of plume height (Carey and Sparks 1986; Pyle 1989) and erupted volume (Pyle 1989; Fierstein and Nathenson 1992; Bonadonna and Houghton 2005; Connor and Connor 2006). For simplicity, discrepancies between two values are calculated as percentage errors and are here defined as *very low* (<10%), *low* (10–20%), *moderate* (20–50%), *large* (50–100%) and *very large* (>100%). This project complements the effort of the IAVCEI Commission on Tephra Hazard Modelling for the standardization of field-based techniques (http://www.ct.ingv.it/Progetti/Iavcei/).

Compilation of isopach and isopleth maps

The compilation of isopach maps relies mainly on the quality of the deposit exposure. In contrast, the compilation of isopleth maps also relies on the definition of maximum clast, which is based on the size characterization of the largest pumices and lithics found in a given outcrop. The implications of such a definition are addressed in the work of the IAVCEI Commission on Tephra Hazard Modelling (report of the 2006 CTHM workshop: Field measurements for the characterization of tephra deposits, http://www.ct.ingv.it/Progetti/Iavcei/report1.htm). Sparks et al. (1981) have shown that the geometric mean of the three axes of the five largest clasts is 1.5 times larger than the value associated with the coarsest 1% of the total grainsize distribution of the 1,875 eruption of Askja volcano (Askja D, Iceland). In this paper we focus on the effects of different averaging techniques on the compilation of isopleth maps and, as a result, on the determination of plume height using the models of Carey and Sparks (1986) and Pyle (1989). Different authors have used different averaging techniques and different sampling strategies for the measurement of the maximum size of clasts and the compilation of isopleth maps (see Fig. 1 and Appendix 1), which inevitably lead to non-unique determinations of plume height. As an example, Barberi et al. (1995) have shown that the average of the maximum axis of the 3 largest clasts collected from a 2-m length exposure and excavating 5 cm of the deposit underestimates the crosswind range of Carey and Sparks (1986) by 20–40% with respect to an isopleth map compiled averaging the maximum axis of the 5 largest clasts sampled over 0.5 m^2 depositional area (i.e. larger sampled volume). Carey and Sparks (1986) have also shown that the estimate of plume height strongly relies on contouring assumptions (i.e. contouring of maximum or average values).

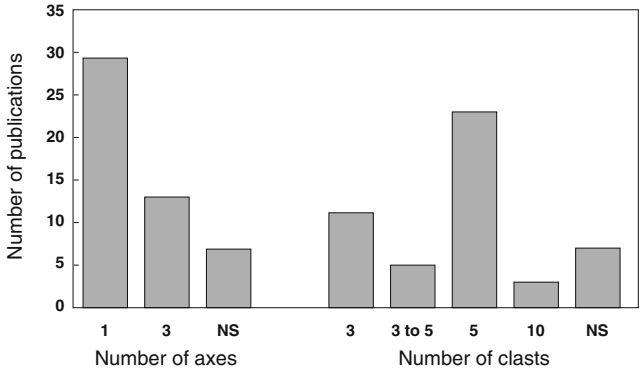

Fig. 1 Frequency of occurrence for different sampling strategies for the measurement of maximum clasts from 48 publications. Only number of clast axes and number of clast measured are indicated. See text for other differences in sampling methods and Appendix 1 for references. *NS* non specified

Isopleth lines presented in this study are based on the contouring of maximum values of the estimate of largest clasts (Carey and Sparks 1986).

Figure 1 and Appendix 1 show how most authors base the compilation of isopleth maps on the mean of the maximum axis of the five largest clasts (29% of all references) and a sampling area of 0.5 m^2 (15%). However, some authors prefer to use an average value of the three main axes of a clast. Both the arithmetic mean and the geometric mean are used to calculate an average axis value, although the arithmetic mean is more commonly used. The use of the geometric mean for the compilation of isopleth maps was firstly introduced by Sparks et al. (1981). In fact, the geometric mean of a given clast represents the diameter of the equivalent sphere and therefore it is considered more suited for the application of empirical models based on the assumption of spherical particles. Regardless of the sampling area, 60% of authors used the 1-axis technique, 27% used the 3-axes technique and 13% did not specify the technique used (Fig. 1). The number of clasts considered to represent the whole population of the outcrop also varies. Most authors considered the five largest clasts (48%), whereas some used three clasts (23%) or three to five clasts (10%). Therefore, the mean value of the maximum axis of three clasts is being used in 25% of the cases, the mean value of the maximum axis of five clasts in 29% of the cases, the mean value of the maximum axis of three to five clasts in 8% of the cases and the mean value of the three main axes of five clasts in 19% of the cases. Finally, 15% of the authors use a depositional sampling area of 0.5 m^2, but this parameter is not specified in most of the cases (65%).

As a result, we have chosen to compile different isopleth maps based on the following averaging techniques (clasts were always sampled from a 0.5 m^2 area): maximum axis of the three (1/3) and the five (1/5) largest clasts; arithmetic mean of three axes of the three (3/3A), five (3/5A), and ten (3/10A) largest clasts; the geometric mean of three axes of the three (3/3G), five (3/5G) and ten (3/10G) largest clasts; the 50th percentile of a population of 20 clasts. Figures 2 and 3 show that our isopach and isopleth maps are consistent with the results of Barberi et al. (1995) with the same observed westward prevailing wind. The dense vegetation did not allow any sampling on the east flank of the cone, so all the lines were closed using the same upwind constraint. Size values for the largest lithic clasts (cm) are specified in Appendix 2 for each outcrop.

The technique of using the 50th percentile of a 20 clasts population (equivalent to the median value) was firstly applied by the IAVCEI Commission on Tephra Hazard Modelling during a January 16–18 2006 pre-conference workshop in Salcedo, Ecuador, associated with the conference Cities on Volcanoes 4 (http://www.ct.ingv.it/Progetti/Iavcei/report1.htm). Several groups of participants were assigned to collect the 20 largest clasts from a single outcrop. When the 20-clast collections for different groups were compared, it was found that while median values were very similar, there was considerable divergence among sizes of largest clasts. Measuring the average of the three axes of the smallest of the tenth largest clasts could thus be an alternative method to the choice of the maximum clast, as it provides more stable results over a given outcrop, it is not affected by the presence of potential outliers and takes less time. As shown by Fig. 3, this technique yields lower

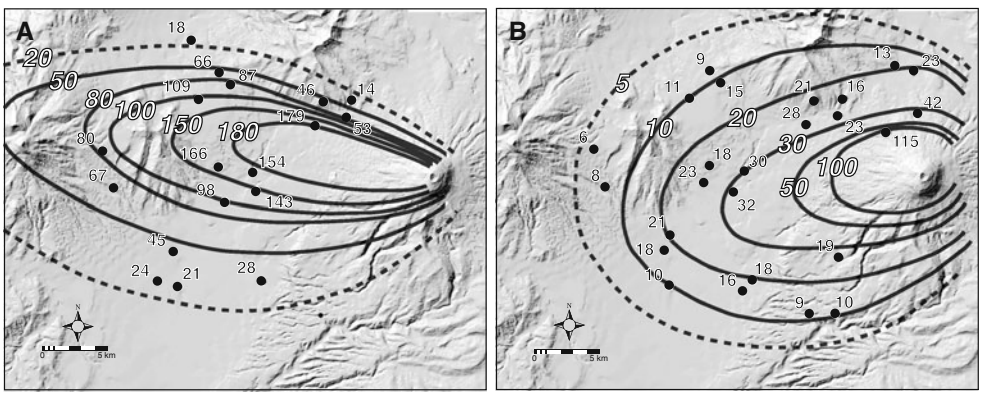

Fig. 2 Isopach maps (in cm) for **a** Layer 3 and **b** Layer 5

values or recorded maximum clast size than do other techniques, and some work still needs to be done in order to calibrate the method. Given that we did not characterize the 50th percentile at all outcrops during our fieldwork, we tested this technique by deriving the ratio between the 50th percentile and the value for 3/5A at the only outcrop where the 50th percentile for both layers 3 and 5 was characterized (see Fig. 3). The ratio of those two techniques on an average of both layers shows that the 50th percentile produces values 23% lower than the 3/5A technique. Assuming that this ratio is maintained at all outcrops, we then calculated the 50th percentile for all other outcrops and compiled isopleth maps for the 50th percentile technique for both layers. As a result, the analysis of the 50th percentile has to be considered as an approximation of individual values, but can provide important general insights on the calibration of this new method.

A comparison of 1-axis and 3-axes techniques reveals only a *low* level of discrepancies (average of both layers, three and five clasts and arithmetic and geometric means), with the 1-axis techniques showing more variable results than the 3-axes techniques (Table 1). The number of clasts considered also has an impact on the shape of the resulting isopleth lines. The levels of discrepancy resulting from the application of the 3/5A technique are *very low* when compared to the 3/3A technique, and *low* when compared to the 3/10A technique. Downwind and half-crosswind ranges decrease with an increasing number of clasts. The impact of the averaging technique (i.e. arithmetic mean vs geometric mean) is relatively limited, and shows *very low* discrepancies for all methods considered. Finally, the 50th percentile of the 20-clasts population shows *low to moderate* discrepancies compared to the 3/5A technique (Fig. 3).

Column height

The heights of the eruptive columns associated with layers 3 and 5 were determined applying both the model of Carey and Sparks (1986) and Pyle (1989) to the isopleth maps shown in Fig. 3. The maximum height above the volcano was determined by subtracting the mean field sampling altitude (i.e. 3,500 m) from the value obtained with these models. The model of Carey and Sparks (1986) is based on the fact that the clast dispersion around the vent mainly depends on the plume height and the wind speed. As a result, the downwind and crosswind ranges of the isopleth maps (i.e. the maximum length and the half width of a given contour) can be used to derive both maximum plume height and wind speed at the time of the eruption. Given that the model of Carey and Sparks (1986) predicts an exponential dependence of clast size on distance from the vent, the decreasing trend of clast sizes with distance from vent can be described by straight lines on semi-log plots of diameter of maximum clasts vs square root of the area of the associated contour. By fitting an empirical function, Pyle (1989) found that the level of neutral buoyancy of the volcanic plumes could be related to the maximum clast half-distance (b_c) for winds lower than 30 m/s.

The model of Carey and Sparks (1986) is based on the geometry of the isopleth contours, whereas the model of Pyle (1989) is based on the area within individual isopleth contours. However, given that the averaging techniques used to compile isopleth maps control both the geometry and the areas associated with a given contour, both models strongly rely on the averaging technique chosen. Figure 4, Appendices 3 and 4 show the spread resulting from the application of Carey and Sparks (1986) to different clast diameters, with the 0.8 and 1.6 cm isopleths showing similar values (*very low* discrepancies—within 3% for all averaging techniques and both layers) and the 3.2 and 6.4 cm isopleths always producing a lower plume height (in the range of *low* discrepancies). Most of our following comparisons are based on the 1.6 cm isopleth line, because it is the only one available for both layers and all averaging techniques. Moreover, to keep our calculations consistent between the two layers and to avoid biasing towards small values, the 10-clasts mean and the 50th percentile techniques were included only where specified. Plume heights inferred with the model of Pyle (1989) for the windy case are always larger than plume heights inferred with the model of Carey and Sparks (1986) (*low* and *very low* discrepancies for layers 3 and 5 respectively, averaged over all techniques and using a mean value of all isopleth lines; grey line in Fig. 4). However, the average of both models gives similar results for all averaging techniques (Table 2). Discrepancies for the plume height indicated by the averaging techniques are *low* and *very low* for the methods of Pyle (1989) and Carey and Sparks (1986) respectively (average of both layers and all isopleth lines; grey line in Fig. 4).

The column height derived with Carey and Sparks (1986) using the 50th percentile shows *low* discrepancies compared to the value obtained using the 3/5A technique (using the 1.6 cm isopleth line only and averaging both layers).

Mass eruption rate (MER)

MER associated with layers 3 and 5 was determined by applying the model of Wilson and Walker (1987). Specifically, we have applied an empirical equation modified for basaltic-andesitic magmas, which are typically characterized by higher temperatures than more silicic plumes and therefore are more buoyant (i.e. we used an empirical

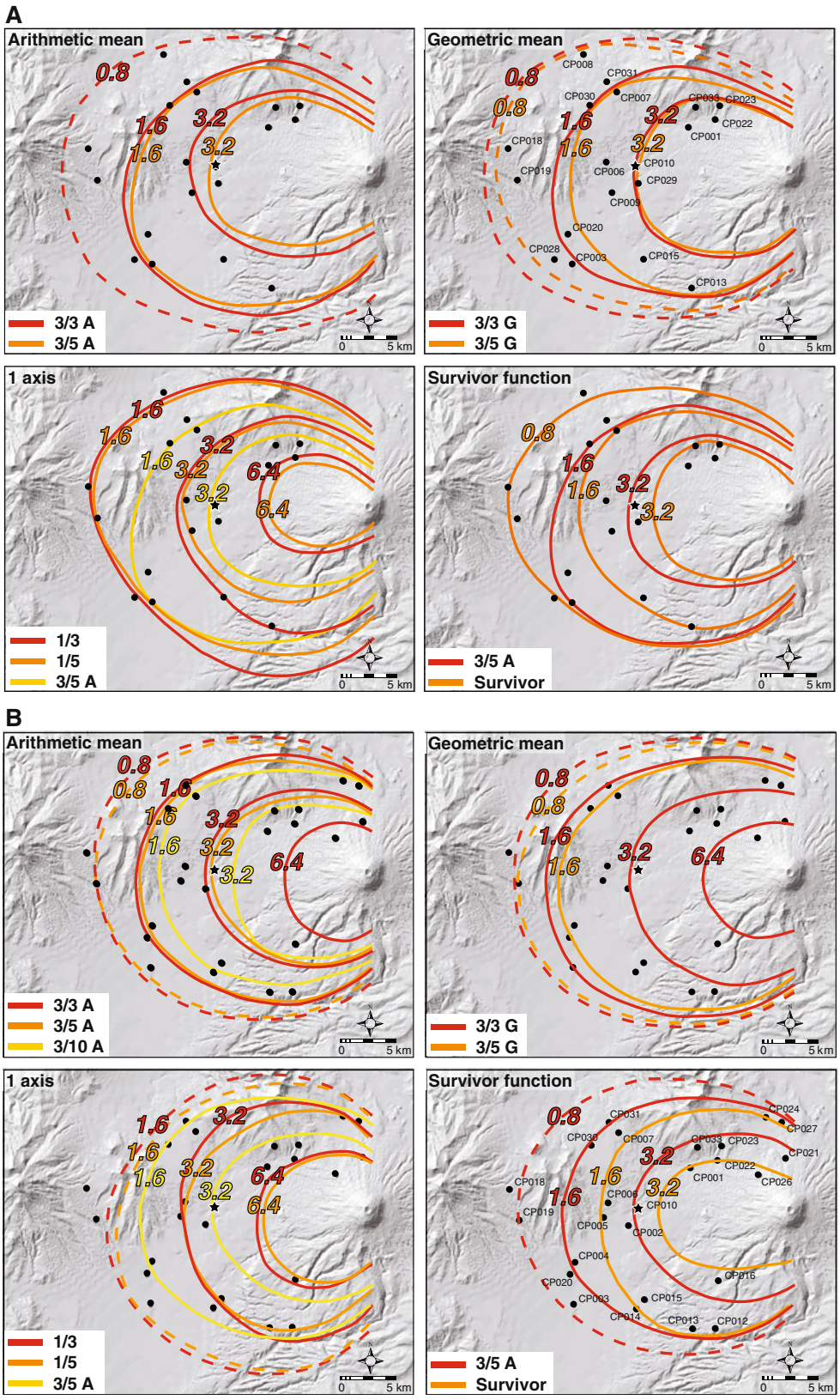

Fig. 3 Isopleth maps (maximum lithics, cm) compiled with the different techniques for **a** Layer 3 and **b** Layer 5. The *dashed lines* are poorly constrained. The *star* shows the outcrop where the 20 clasts for 50th percentile technique have been measured

Table 1 Downwind (DW) and crosswind (CW) ranges (in km) as defined by Carey and Sparks (1986) for the 1.6 cm isopleth line compiled using different averaging techniques

	1/3		1/5		3/3A		3/5A	
	DW	CW	DW	CW	DW	CW	DW	CW
Layer 3	25.2	13.2	24.8	11.9	21.8	11.4	23.3	10.8
Layer 5	23.3	13.4	22.5	12.8	20.6	11.3	20.3	11.0

constant of 0.295 as supposed to 0.236; Costantini et al. 2009).

Figure 5, Appendices 3 and 4 show that discrepancies of MER associated with plume height derived using different averaging techniques are *moderate* for the method of Pyle (1989) and Carey and Sparks (1986) applied to the 1.6 cm line, and *large* for the method of Carey and Sparks (1986) applied to the 3.2 cm line (average of both layers). The average discrepancy between MER derived from plume heights based on the method of Carey and Sparks (1986) and Pyle (1989) is *moderate* for both layers (average of all isopleth lines; grey line in Fig. 5). Finally, comparing MER derived from the 0.8 and 1.6 cm lines with those derived from the 3.2 and 6.4 cm lines results in a range of *low* to *large* discrepancies (Carey and Sparks 1986), including both layers and all averaging techniques. In general, discrepancies in the plume height result in 70% higher discrepancies in the MER. MER inferred based on the 50th percentile is smaller (*moderate* discrepancies) than the MER based on the 3/5A technique (using the 1.6 cm isopleth line only and averaging both layers).

Erupted volume

The determination of erupted volume is typically based on the information retained within the isopach maps. However, given that the data acquisition for isopach maps is of less complexity than for isopleth maps, we focused our uncertainty analysis on the application of different models. In particular, we have applied the model of Pyle (1989), based on the assumption of exponential thinning of one segment, the model of Fierstein and Nathenson (1992) based on the exponential thinning of two segments, the model of Bonadonna and Houghton (2005), based on the assumption of power-law thinning and the analytical solution of Connor and Connor (2006). The model of Pyle (1989) is based on the preliminary observation of

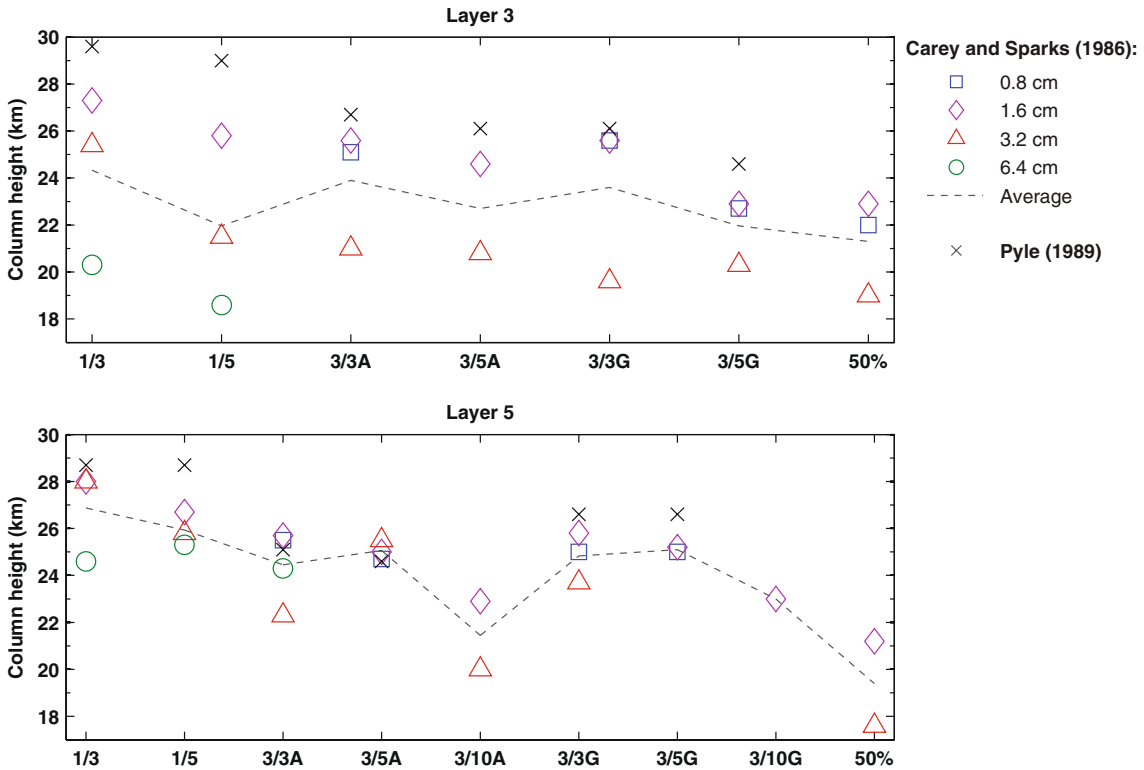

Fig. 4 Column heights (Ht) obtained with the method of Carey and Sparks (1986) for the 0.8, 1.6, 3.2 and 6.4 cm isopleth lines and the method of Pyle (1989). The *grey line* shows the mean of all values derived from Carey and Sparks (1986) method

Table 2 Average values of column height (km) as derived by applying the methods of Carey and Sparks (1986) and Pyle (1989) to all isopleth maps of Fig. 3. The error range is the median of the difference between the maximum (Pyle 1989) and the minimum (Carey and Sparks 1986) values[a] Only Carey and Sparks (1986)

	Layer 3	Layer 5
1/3	27±3	28±1
1/5	25±4	27±1
3/3A	25±1	25±0
3/5A	24±2	25±0
3/10A	–	22[a]
3/3G	25±1	26±1
3/5G	23±1	26±1
3/10G	–	23[a]
50th%	21[a]	20[a]

Thórarinsson (1954) that both thickness and grainsize of tephra deposits mostly follow an exponential decay with distance from the vent. However, analytical models and detailed field studies have recently shown that the thinning of well-preserved deposits can be either described by four exponential segments or by a power-law fit on a semi-log plot of thickness vs square root of isopach areas (Pyle 1995; Bonadonna et al. 1998; Bonadonna and Houghton 2005). Although both methods are based on empirical curve fitting of field data plotted on semi-log plots of thickness vs square root of the area of the corresponding isopach contour, they can yield very different values for erupted volume. In particular, the exponential method applied to poorly exposed deposits can significantly underestimate the erupted volume, whereas the power-law method applied to widely dispersed and not well-exposed deposits can significantly overestimate the volume (Bonadonna and Costa 2010). Both methods must therefore be applied with care.

Our dataset includes 6 isopach lines for Layer 3 (180, 150, 100, 80, 50, 20 cm) and 6 for Layer 5 (100, 50, 30, 20, 10, 5 cm), which represents mainly the medial deposit (Fig. 2). The lack of proximal data is due to the ice cap on the summit of the Cotopaxi volcano, which has also resulted in generation of numerous lahars and, therefore, reworking of proximal deposits, whereas the distal deposit is not preserved or is covered by vegetation. Only one straight segment is evident for Layer 3, whereas we could also identify a more proximal segment for Layer 5 (Fig. 6).

As expected, volumes calculated with the power-law method are larger than those calculated with the exponential technique (Table 4). The volume resulting from the exponential technique applied to the two segments of Layer 5 is 29% larger than the volume resulting from the integration of only one segment. Finally, the volume associated with Layer 3 is more sensitive to the choice of the distal extreme of integration required by the power-law technique than the volume associated with Layer 5. This is due to the fact that Layer 3 is more widely dispersed than Layer 5, which results in different power-law exponents (1.76 and 2.11 respectively). Bonadonna and Costa (2010) have shown that the application of the power-law method to

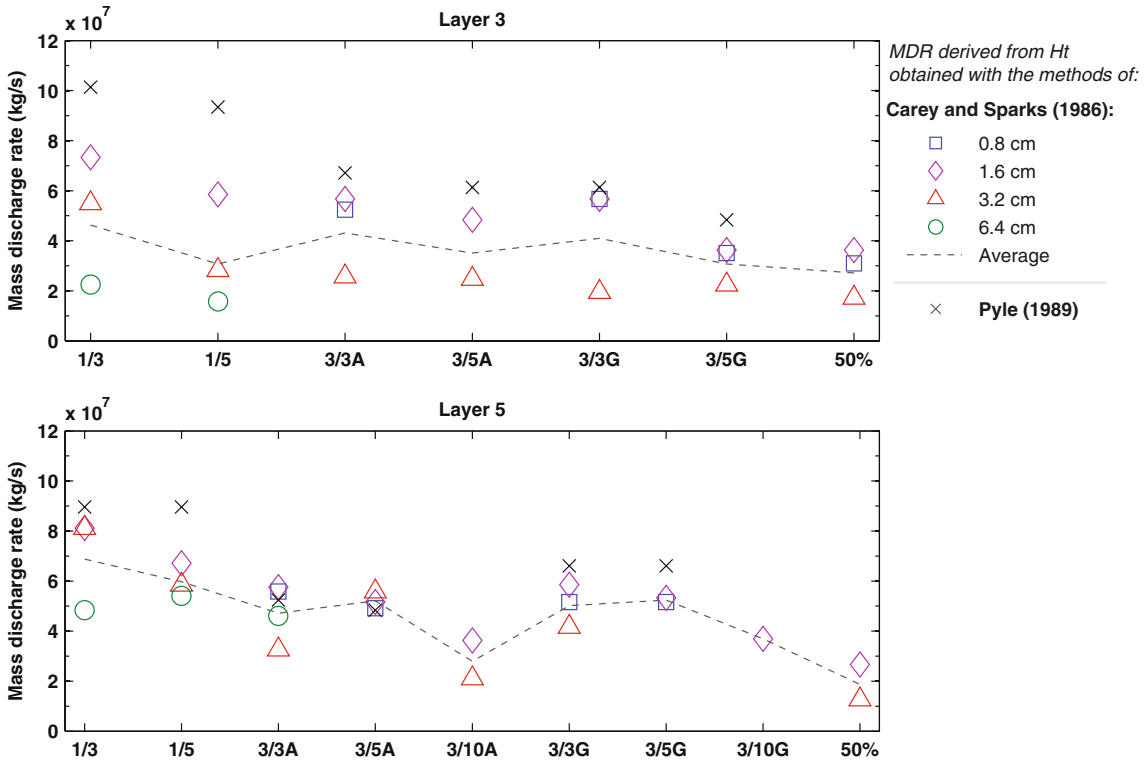

Fig. 5 Mass eruption rates calculated using the method of Wilson and Walker (1987) adapted for basaltic–andesitic eruptions, for all column heights obtained in Fig. 4. The *grey line* shows the mean of all values derived from the method of Carey and Sparks (1986)

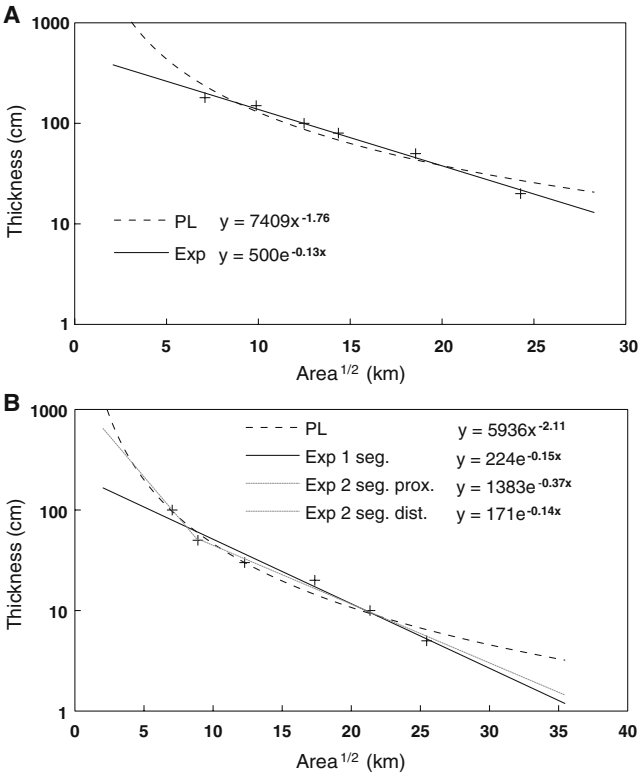

Fig. 6 Semi-log plots of thickness vs square root of area for **a** Layer 3 and **b** Layer 5. Different best-fit curves and associated equations are also shown: 1 exponential segment (*solid black line*), 2 exponential segments (*solid grey line*) and power-law (*dashed black line*)

tephra deposits with power-law exponents <2 is problematic and characterized by larger uncertainties.

The erupted volume can also be derived from the analytical inversion of field data, which bypasses the issue of data contouring. In particular, analytical models for tephra dispersal can be combined with inversion strategies in order to determine specific eruptive parameters. As an example, we have applied the method of Connor and Connor (2006) based on the combination between the advection–diffusion model TEPHRA2 (Bonadonna and Houghton 2005; Connor and Connor 2006) and the downhill simplex method to find the optimized set of eruptive parameters to describe a given tephra deposit. The optimized set of parameters is determined by the goodness of fit between observed and computed mass accumulation per unit area, which is determined on the basis of the root mean square error (RMSE). Figure 7 shows a minimum in the RMSE (dark brown zones) for a mass between 1.4–1.7×10^{12} and 0.6–1.1×10^{12} for Layer 3 and Layer 5 respectively (within 20% RMSE variation). Inversion runs were carried out first for plume heights ranging between 20 and 36 km (2 km steps) and erupted mass between 10^{10}–10^{14} kg for Layer 3 and 10^{10}–10^{13} kg for Layer 5. Our results confirm that the erupted mass can be better constrained than the plume height, as already shown by Volentik et al. (2010) and Bonadonna and Costa (2010). A second set of runs was carried out using refined ranges of eruptive parameters. Based on empirical results, plume heights were reduced to a range of 25–35 km, and the range of erupted mass was reduced between 0.5–10×10^{12} kg and 0.1–5×10^{12} kg for Layer 3 and Layer 5 respectively (based on previous inversion analysis). Results are an erupted mass of 1.7×10^{12} kg for Layer 3 (with a corresponding column height of 29 km) and 0.6×10^{12} kg for Layer 5 (with a corresponding column height of 32 km) which can be converted into volumes of 2.4 km^3 and 0.5 km^3 for Layer 3 and Layer 5 respectively (Table 4). Resulting plume heights are in good agreement with the empirical results shown in Table 2. Erupted masses were converted to erupted volumes using bulk densities of 700±24 kg/m^3 and 950±85 kg/m^3 for layers 3 and 5 respectively as measured in the field.

Duration

The duration of volcanic events is an important parameter in the field of risk assessment, but often difficult to derive. Estimates of past eruption durations can be valuable inputs for forecasts of future activity. We quantified the variability of eruption durations as calculated from the combination of MER (Fig. 5, Table 3) and erupted mass resulting from the application of both empirical (Pyle 1989; Fierstein and Nathenson 1992; Bonadonna and Houghton 2005) and analytical models (Connor and Connor 2006) (Table 4).

Figure 8 and Table 5 show the eruption duration values calculated from the mean MER obtained from plume heights derived using Pyle (1989) and Carey and Sparks (1986). Durations derived from plume heights calculated with the method of Carey and Sparks (1986) applied to the 0.8 and 1.6 cm isopleth lines show *very low* discrepancies with the duration averaged for all values of plume height and mass. Minimum and maximum durations of eruption were calculated by combining the highest and lowest values of MER and erupted mass, i.e. Pyle (1989) for plume height and the exponential 1-segment method for the erupted volume (minimum), and Carey and Sparks (1986) for plume height and the power-law method with $\sqrt{A_{dist}} = 500\,\mathrm{km}$ for the erupted volume (maximum). Discrepancies between minimum and maximum durations are *large* to *very large*, for both layers and compared both with analytically and empirically derived masses.

Eruption classification

Explosive eruptions can be classified by eruption style based on quantitative thinning and grainsize parameters (Walker 1971; Pyle 1989), magnitude and intensity scales

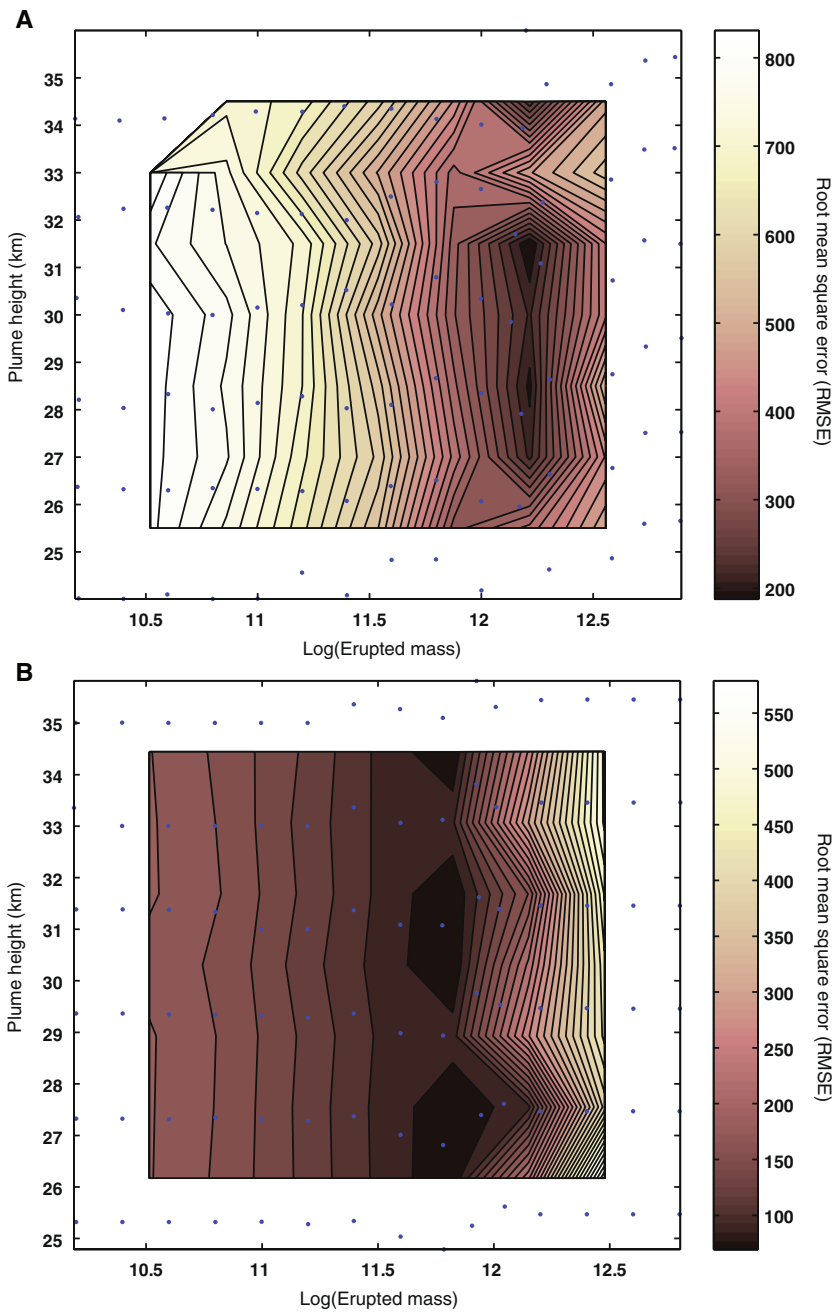

Fig. 7 Analytical solutions of the inversion model of Connor and Connor (2006) for **a** Layer 3 and **b** Layer 5. The *color bar* on the left represents the Root Mean Square Error. *Blue dots* are the different runs. *Dark brown zones* are best-fit values, showing a better constrain of the erupted mass than the column height

(Pyle 2000) and Volcanic Explosivity Index (VEI; Newhall and Self 1982). However, all methods strongly rely on field data and therefore do not always give unique answers. Figure 9 shows that both layers are at the limit between subplinian and Plinian activities, with the 1-axis technique resulting in a lower b_c/b_t ratio. In fact, both layers are classified as Plinian based on the 1-axis technique and subplinian based on the 3-axes technique (Fig. 9). Intensity and magnitude indices derived from all MER and erupted masses vary between 10.6 and 11.2 and between 4.3 and 5.2 respectively (*very low* discrepancies; Tables 6 and 7). Figure 10 shows that the VEI classes can vary depending on the technique chosen for the calculation of erupted volume. As an example, Layer 3 has a VEI 4 when the volume is calculated with the exponential technique and VEI 5 when power-law and inversion techniques are used.

Discussion

Determination of eruptive parameters

Our results confirm the difficulty of deriving unambiguous values for eruptive parameters such as plume height,

Table 3 Values of mass eruption rate ($\times 10^7$ kgs^{-1}) calculated with the method of Wilson and Walker (1987) adapted for basaltic–andesitic eruptions and applied to values in Table 2

	Layer 3	Layer 5
1/3	7.6±2.6	8.0±1.0
1/5	6.4±3.0	7.5±1.5
3/3A	5.6±1.1	5.0±2.2
3/5A	4.9±1.2	5.0±1.9
3/10A	–	1.4
3/3G	5.3±0.9	5.8±0.8
3/5G	4.0±0.9	5.9±0.7
3/10G	–	1.8
50th%	1.4	1.0

erupted volume, MER and eruption duration. This is because different sampling and data-processing strategies are used to characterize tephra deposits, and different empirical and analytical models are applied to determine eruptive parameters. In addition, even individual models can result in a range of values as opposed to an absolute value (e.g. application of the method of Carey and Sparks (1986) to different isopleth lines for the determination of plume height). Given that different strategies of data processing and different models are based on different assumptions, it is important to have a critical analysis of their application based on the type of deposit/eruption considered and on the purpose of the analysis. As an example, the method of Carey and Sparks (1986) should only be applied to products of sustained eruptions because it is based on plume velocities typical of Plinian eruptions. Even for sustained eruptions, it is still more realistic to provide for a given tephra deposit, and therefore a given eruptive event, a range of values for plume height, erupted volume, MER and eruption duration more than a single value. In fact, though we can recommend optimal field strategies and data-processing techniques to be used, the use of any single empirical model for the determination of eruptive parameters can provide misleading results.

Table 4 Summary of volumes (km^3) obtained with the different techniques described in the text. For the power-law technique (Bonadonna and Houghton 2005), the proximal integration limit $\sqrt{A_0}$ is 5.1 km for Layer 3 and 4.3 km for Layer 5

		Layer 3	Layer 5
Exponential (Pyle 1989)	1 segment	0.6	0.2
	2 segments		0.3
Power-law (Bonadonna and Houghton 2005)	$\sqrt{A_{dist}} = 100$ km	1.0	0.3
	$\sqrt{A_{dist}} = 300$ km	1.5	0.3
	$\sqrt{A_{dist}} = 500$ km	1.9	0.3
Inversion (Connor and Connor 2006)		2.4	0.5

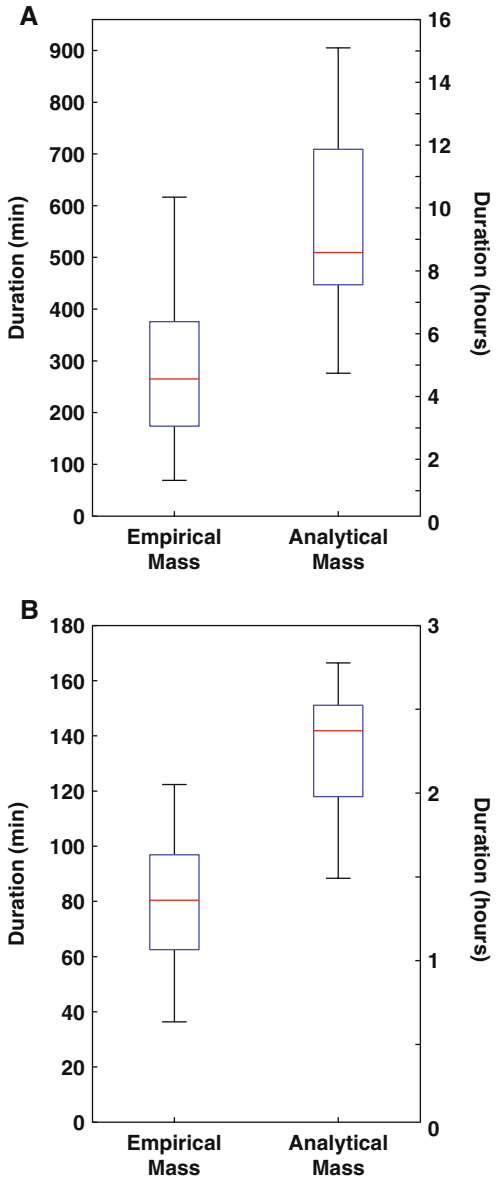

Fig. 8 Eruption durations for the two layers for **a** Layer 3 and **b** Layer 5, calculated with masses from both empirical and analytical methods and mass discharge rates from all techniques of determination of column heights, except the 50th percentile of the survivor function. The *box* shows the 25th and 75th percentiles, the line inside is the median, and the whiskers are the minimum and maximum values

Data processing vs dispersal models

A reliable characterization of eruptive events always starts with a thorough characterization of tephra deposits, which is based on a good sampling strategy. The application of empirical and analytical models for the determination of eruptive parameters relies on good deposit exposure and a uniform distribution of field data, which is not always

Table 5 Eruption duration (min) derived by dividing erupted mass by mass eruption rate. Results obtained using values of erupted mass derived from empirical (Fierstein and Nathenson 1992; Pyle 1989; Bonadonna and Houghton 2005) and analytical (Connor and Connor 2006) models are shown. Mass eruption rate is determined with the method of Wilson and Walker (1987) from plume heights calculated following Carey and Sparks (1986) and Pyle (1989). Duration is expressed as mean value±standard deviation

	Layer 3		Layer 5	
	Empirical mass	Analytical mass	Empirical mass	Analytical mass
Pyle (1989)	241±104	381±87	71±22	121±31
Carey and Sparks (1986)	391±171	758±130	85±20	145±19
Mean duration	295±155	570±195	80±21	134±25

possible due to logistical constraints (e.g. erosion, reworking, vegetation cover, sedimentation in the ocean, steep topography). The influence of the distribution of field data on the determination of eruptive parameters is beyond the scope of this paper. Here, we have focused on how data processing and the application of different dispersal models affect the characterization of explosive volcanic eruptions. We have shown that differences among sampling techniques and in data processing can result in larger discrepancies in calculated plume heights than does the application of different dispersal models. As an example, the 1.6 cm isopleth line of Layer 5 shows a 16% variation in calculated plume heights resulting from the use of different techniques for calculating largest clast sizes for isopleth construction (here between the 1/3 and 3/10G techniques; Fig. 4), whereas the discrepancy resulting from the use of different empirical models (Carey and Sparks 1986; Pyle 1989) is only 5% (considering Layer 5 and using all isopleth lines). In applying the model of Carey and Sparks (1986) the error range resulting from the use of the different isopleth lines is 20% and 6% for layers 3 and 5 respectively.

Still using the 1.6 cm isopleth line only, the 1-axis averaging techniques (1/3, 1/5) results in a 5% and 6% discrepancy with respect to the 3-axis techniques (3/3A, 3/5A) for layers 3 and 5 respectively. The use of geometric mean as opposed to the arithmetic mean of the 3-axes (3/3A, 3/5A vs 3/3G, 3/5G) only results in a discrepancy of 3% and 1% for layers 3 and 5 respectively. The number of clasts considered (3/3A, 3/3G vs 3/5A, 3/5G) results in a discrepancy of 6% and 2% for layers 3 and 5 respectively. Ten clasts were only available at a few outcrops of Layer 5 and show a discrepancy of 9% with respect to the 3-clast technique.

We consider that standardization of field strategies and data processing to characterize the "maximum clast size" used in isopleth construction has become crucial. Considering that the maximum clast is used in a dispersal model that is based on the assumption of spherical particles (Carey and Sparks 1986), a clast characterization based on the geometric mean of the three orthogonal axes should be favored. The use of the 50th percentile introduced by the IAVCEI Tephra Commission represents a good alternative because it eliminates the problem of outliers and results in a more stable characterization across a certain outcrop than the average of a few clasts. However, the use of the 50th percentile for the determination of plume height still needs to be accurately calibrated with the method of Carey and Sparks (1986) before it can be safely applied. By definition, the 50th percentile would return lower values of plume heights as it is associated with lower values of largest clasts. As an example, the 50th percentile applied to the 1.6 cm isopleth line results in a plume height that is 6% and 13% lower than the plume height derived from the 3/5A technique for layers 3 and 5 respectively.

In addition, our results confirm that the application of the method of Carey and Sparks (1986) to the 6.4 and 3.2 cm

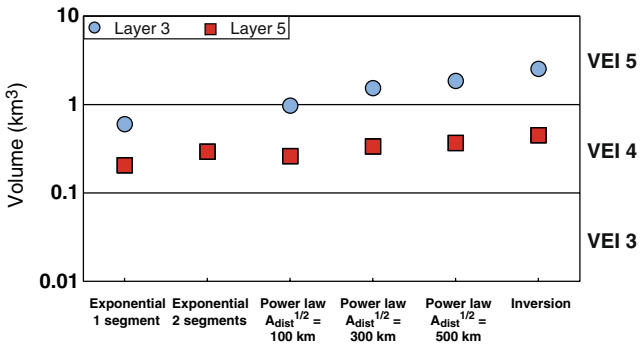

Fig. 9 Eruptions styles as defined by Pyle (1989), based on thickness and maximum clast half-distances

Table 6 Intensity index calculated with the method of Pyle (2000) and mass eruption rates from Table 3, where intensity = $\log_{10}$(MER [kg/s])+3

	Layer 3	Layer 5
1/3	11.1±0.1	11.1±0.1
1/5	11.0±0.2	11.1±0.1
3/3A	11.0±0.1	11.0±0.1
3/5A	11.0±0.1	10.9±0.1
3/10A	–	10.8[a]
3/3G	11.0±0	11.0±0
3/5G	10.8±0.1	11.0±0
3/10G	–	10.8[a]
50th%	10.8[a]	10.6[a]

[a] No information from Pyle (1989)

Table 7 Magnitude index calculated with the method of Pyle (2000) and erupted masses from Table 4, where magnitude = $\log_{10}$(erupted mass [kg])−7

		Layer 3	Layer 5
Exponential (Pyle 1989)	1 segment	4.6	4.3
	2 segments		4.5
Power-law (Bonadonna and Houghton 2005)	$\sqrt{A_{dist}} = 100$ km	4.8	4.5
	$\sqrt{A_{dist}} = 300$ km	5.0	4.5
	$\sqrt{A_{dist}} = 500$ km	5.1	4.5
Inversion (Connor and Connor 2006)		5.2	4.7

NS non specified, *AM* arithmetic mean, *GM* geometric mean

isopleth lines results in lower plume heights than the application to the 1.6 and 0.8 cm isopleths as already shown by Papale and Rosi (1993) and Rosi (1998). The 3/3A technique for Layer 5 is the only case where all isopleth lines are available (see Fig. 3) and shows that column heights calculated from the 3.2 and 6.4 cm isopleth lines are 8% lower than those resulting from calculations on the 0.8 and 1.6 cm. In fact, the sedimentation of the 6.4 and 3.2 cm clasts is more likely to be affected by the complex plume dynamics than the sedimentation of the 1.6 and 0.8 cm clasts, which are typically carried up to the umbrella cloud. As a result, we consider the application of the method of Carey and Sparks (1986) to the 1.6–0.8 cm clasts more reliable than its application to the 6.4–3.2 cm clasts.

The application of different dispersal models for the determination of erupted mass can result in even larger discrepancies than for the determination of plume height (Table 5). The percentage difference of the volume calculated by integrating one exponential segment versus the application of inversion techniques is 75% and 60% for Layer 3 and Layer 5 respectively. Similarly, volumes resulting from the power-law method with a distal integration limit of 300 km are 38% and 40% smaller than those obtained with the inversion techniques (for Layer 3 and Layer 5 respectively). The application of the method of Connor and Connor (2006) is expected to be more reliable for the determination of erupted mass because it bypasses the data-contouring steps and because it is based on a physical model for the description of tephra dispersal as opposed to empirical extrapolations of field data (Pyle 1989; Fierstein and Nathenson 1992; Bonadonna and Houghton 2005). However, apart from requiring a more sophisticated computation than the application of empirical models, a sensitivity analysis of such a strategy as applied to a range of data distributions and eruptive styles still needs to be carried out. We note that the application of inversion techniques to grainsize data, rather than to mass/area data, seems to lead to a better constrain of both erupted mass and plume height (Volentik et al. 2010).

Propagation of error and reproducibility of results

Given that MER and the duration of the sustained phase of an eruption are typically derived from the calculated plume height and the erupted mass, it is important to investigate the effect of error propagation. MER is related to the 4th-power of the plume height. As a result, considering Layer 5 only, the average discrepancies in the estimate of plume height related to data processing of the 1.6 cm isopleth line (16%) leads to an average discrepancy of 50% in the estimate of MER, whereas the average discrepancy related to the application of different dispersal models (5%) leads to a MER discrepancy of 20%. Our study is limited to the application of the model of Wilson and Walker (1987) for the derivation of the MER, and different discrepancies would result if applying different models (e.g. Sparks 1986), even though the fourth-power relationship exerts the major control on error propagation. If we combine the discrepancies in calculated MER with the discrepancies associated with the determination of the erupted mass, we find a maximum discrepancy in the determination of the eruption duration of 84% (ignoring values derived from

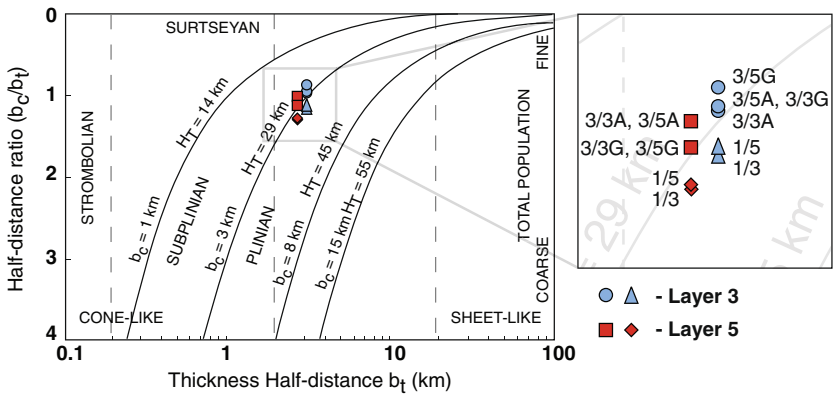

Fig. 10 VEI plot modified from Newhall and Self (1982)

the inversion technique of Connor and Connor 2006). In order to minimize discrepancies in the determination of plume height and MER, a standard characterization of tephra deposits should be introduced. In particular, even though we should still provide a range of parameters based on the application of different dispersal models, an effort should be made to adopt a standard technique for the determination of the largest clasts.

Eruption classification

Eruption classification may be based on the variation of maximum clast-size and deposit thinning with distance from the vent and on the erupted volume (Newhall and Self 1982; Pyle 1989, 2000), and is therefore affected by the field sampling technique adopted.

Figure 9 shows how both Layer 3 and Layer 5 are classified as Plinian based on the 1-axis technique and as subplinian based on the 3-axis technique for the compilation of isopleth maps. Similarly, Figure 10 shows how Layer 3 can be classified as VEI 4 or 5 depending on the model used to derive the erupted mass (Fig. 10).

Volcanic eruptions can also be compared through the use of the magnitude and intensity scales (Pyle 2000), which are based on the erupted mass and the MER respectively. Even though both the VEI classification and the magnitude index have logarithmic scales, the magnitude index is continuous and therefore provides a better characterization of the variability of erupted volume. By using all values of erupted mass and MER, the variability in both calculated magnitude and calculated intensity shows *moderate* to *large* discrepancies.

Conclusions

A comprehensive characterization of explosive eruptions relies on a detailed study of tephra deposits. Based on our systematic investigation of Layer 3 and Layer 5 of Cotopaxi volcano, we can conclude that:

1. Explosive volcanic eruptions are better characterized by a range of values for plume height, MER, erupted volume and eruption duration derived by the application of different dispersal models as supposed to a single set of absolute values.
2. The range in calculated plume heights is <20% for all averaging techniques and models used.
3. The determination of plume height from isopleth maps is more sensitive to the averaging technique used to compile isopleths maps than to the choice of dispersal models considered (e.g., Carey and Sparks 1986; Pyle 1989).
4. 1-axis averaging techniques overestimate plume heights by 6% with respect to 3-axis techniques (average of both layers).
5. 3-clast averaging techniques overestimate plume heights by 2% with respect to 5-clast techniques and by 9% with respect to 10-clasts techniques (Layer 5 only).
6. Plume heights derived applying the method of Pyle (1989) are 9% higher than plume heights derived applying the method of Carey and Sparks (1986) (average on both layers).
7. Plume heights derived applying the method of Carey and Sparks (1986) on the 3.2 and 6.4 cm isopleth lines are 10% lower than plume heights derived using the method of Carey and Sparks (1986) on the 0.8 and 1.6 cm isopleth lines (average of both layers).
8. In our case study, the erupted mass derived from inversion techniques is typically larger than the erupted mass derived from empirical fits.
9. Determination of MER is related to the 4th power of the plume height. Average discrepancies for both layers associated with clast-size averaging techniques and different dispersal models are within 50% and 20% MER discrepancies respectively.
10. Calculated eruption duration relies on the determination of both MER and erupted mass and shows an average final discrepancy of about 40% (average of both layers).
11. Eruption classification based both on the erupted mass (VEI) and on the distribution of maximum clasts (Pyle 1989) is sensitive to the choice of the dispersal model used and to the compilation of isopleth maps. In contrast, magnitude and intensity indexes provide more consistent results.

Based on our results, we recommend that:

- Averaging techniques and sampling areas considered for the compilation of isopleth maps should be standardized in order to reduce the large variations in modeled plume height that result from different clast-size measurement strategies, which then feed through via MER to estimates of eruption duration and to eruption classification.
- The physical constrain of intense eruptions (i.e. eruptions associated with widespread tephra fall deposits) should be used to constrain the integrated application of different empirical and analytical models. Intense and large-magnitude eruptions are more difficult to characterize in terms of erupted mass and eruption classification than are small eruptions.

Acknowledgements We are grateful to Bruce Houghton and David Pyle for their reviews, to Raffaello Cioni, Licia Costantini, Marco Pistolesi, Mauro Rosi and Kae Tsunematsu for their enthusiastic support and constructive discussion in the field, to Bruce Houghton for his contribution in the literature review and to Flora Boekhout for her help in the data processing. Costanza Bonadonna was supported by the Swiss National Science Foundation Grant 200021-116335.

Appendix 1

Table 8 Literature review of some publications using the concept of isopleth maps and their method used to measure maximum clasts

Reference	Volcano, Formation	Date/Age	Method	Numb. Axis	Numb. Clasts	Sampling area
Walker and Croasdale 1971	Agua de Pau	4600 B.P. and 1563 A.D.	NS	1	3	NS
Lirer et al. 1973	Somma-Vesuvius	79 A.D. and 3.5 Ka	NS	1	3	NS
Suzuki et al. 1973	Tarumai, Ta-b	1667 A.D.	NS	1	10	1 m^2
Self 1976	Terceira Group	Recent activity	NS	1	3	NS
Walker 1980	Taupo, Taupo Pumice	1820 B.P.	NS	1	3	NS
Sparks et al. 1981	Askja	1875	GM	3	5	1 m^2
Walker 1981	Taupo, Waimihia and Hatepe	3400 and 1850 B.P.	NS	1	3	NS
Sigurdsson et al. 1982	Vesuvius	79 A.D.	NS	1	5	1 m^2
Williams and Self 1983	Santa-Maria	October 1902	NS	1	3	NS
Walker et al. 1984	Tarawera	1886	NS	1	3	NS
Carey and Sigurdsson 1986	El Chichon	1982	NS	1	5	0.5 m^2
Carey and Sigurdsson 1987	Vesuvius	79 A.D.	NS	1	5	NS
Kanisawa and Yoshida 1989	Adachi, Adachi-Medeshima Pumice Deposit	Late Pleistocene	NS	1	3	NS
Sigurdsson and Carey 1989	Tambora	1815	NS	1	5	NS
Carey et al. 1990	Mt. St. Helen	May 18, 1980	NS	1	5	0.5 m^2
McPhie et al. 1990	Kilauea	1790	NS	NS	NS	NS
Limburg and Varekamp 1991	Nisyros	44–24 ka	AM	3	10	NS
Fierstein and Hildreth 1992	Novarupta	1912	AM	3	3 to 5	1–25 m^2
Hildreth and Drake 1992	Quizapu	10–11 April 1932	AM	3	3 to 5	NS
Papale and Rosi 1993	Pululagua	2450 B.P.	NS	1	5	0.5 m^2
Rosi et al. 1993	Vesuvius	1631	NS	1	5	0.5 m^2
Wilson 1993	Taupo	Late Quaternary	NS	1	5	NS
Scasso et al. 1994	Hudson	August 12–15, 1991	AM	3	NS	NS
Ablay et al. 1995	Montaña Blanca	~2 ka	AM	3	5	NS
Barberi et al. 1995	Cotopaxi	Last 5000 years	NS	1	3 to 5	0.5 m^2
Cole et al. 1995	Furnas	1630 A.D.	NS	NS	NS	NS
Giannetti 1996	Roccamofina	274 ka	NS	1	3	NS
Palladino and Agosta 1997	Vulsini Volcanic District	0.3–0.2 Ma	NS	1	5	2 m long section
Naranjo and Stern 1998	Hudson	Holocene	NS	NS	NS	NS
Rolandi et al. 1998	Somma-Vesuvius	Last 3500 years	AM	3	5	NS
Rosi et al. 1999	Phlegraean Fields caldera, Campanian Ignimbrite	36 ka	AM	3	5	0.5 m^2
Bryan et al. 2000	Las Cañadas, Granadilla Member	0.57 Ma	AM	1	5	NS
Gardner and Tait 2000	Ceboruco	1000 B.P.	AM	3	5	NS
Giannetti and De Casa 2000	Roccamofina, White Trachitic Tuff	317–230 Ma B.P.	AM	NS	3	tens of m^2
Luhr 2000	San Juan, Tepic Pumice	14 770 B.P.	NS	1	3 to 5	NS
Adams et al. 2001	Huaynaputina	1600 A.D.	NS	1	3 to 5	variable
Jurado-Chichay and Walker 2001	Okataina volcanic center, Mangaone Subgroup	31 to 43 ka	NS	NS	NS	NS
Andronico and Cioni 2002	Vesuvius, Avellino and Pompeii eruptions	3.5 Ka - 79 A.D.	NS	1	5	0.1 m^3 (volume)
Rodríguez et al. 2002	Las Cumbres Volcanic Complex, Quetzalapa Pumice	20 ka	AM	3	5	1 m^2
Thouret et al. 2002	Huaynaputina	1600 A.D.	NS	1	10	>1 m^2
Cioni et al. 2003	Somma-Vesuvius, Greenish Pumice	16 020±130 B.P.	AM	3	5	NS

Table 8 (continued)

Reference	Volcano, Formation	Date/Age	Method	Numb. Axis	Numb. Clasts	Sampling area
Milner et al. 2003	Taupo, Mamaku Ignimbrite	220–230 ka	NS	3	5	NS
Rolandi et al. 2004	Somma	472 A.D.	NS	1	5	NS
Sottili et al. 2004	Sabatini Volcanic District	514–449 ka	NS	1	5	NS
Pérez et al. 2006	Barva Caldera, Tirbi Tuff	322 ka	NS	NS	NS	NS
Rossotti et al. 2006	Citlaltèpetl, Citlaltèpetl Pumice	9.0–8.5 ka	NS	1	5	0.5 m^2
Wehrmann et al. 2006	Massaya volcanic area, Fontana Tephra	~60 ka	AM	3	5	NS

Appendix 2

Table 9 Value of largest lithics (cm) for A) Layer 3 and B) Layer 5

Outcrop	1/3	1/5	3/3A	3/5A	3/10A	3/3G	3/5G	3/10G	50%
A									
CP001	5.77	5.48	4.38	4.11	–	4.26	3.99	–	3.20
CP003	2.67	2.42	1.76	1.61	–	1.57	1.42	–	1.25
CP006	4.70	4.18	3.17	2.99	–	2.97	2.81	–	2.33
CP007	2.97	2.72	2.17	2.01	–	2.02	1.88	–	1.57
CP008	1.27	1.20	0.98	0.92	–	0.93	0.87	–	0.72
CP009	3.27	3.12	2.20	2.11	–	2.04	1.96	–	1.65
CP010	5.03	4.76	3.39	3.23	2.99	3.23	3.07	2.74	2.52
CP013	3.33	2.74	2.36	2.02	0.00	2.23	1.92	–	1.58
CP015	3.17	2.82	2.38	2.16	1.93	2.33	2.11	1.86	1.68
CP018	1.63	1.52	1.13	1.07	–	1.03	0.96	–	0.83
CP019	1.83	1.76	1.21	1.19	–	1.15	1.11	–	0.93
CP020	2.07	1.90	1.48	1.37	–	1.38	1.27	–	1.07
CP022	6.67	5.90	4.84	4.47	–	4.71	4.31	–	3.49
CP023	6.03	5.52	4.11	3.79	3.13	3.75	3.48	2.91	2.95
CP028	1.53	1.46	1.06	1.00	0.89	0.96	0.91	0.83	0.78
CP029	5.33	5.22	4.02	3.87	3.46	3.90	3.69	3.29	3.02
CP030	2.47	2.22	1.59	1.47	1.34	1.42	1.32	1.21	1.14
CP031	2.07	1.98	1.40	1.34	1.22	1.30	1.22	1.10	1.05
CP033	5.97	5.72	4.44	4.22	3.82	4.25	4.04	3.61	3.29
B									
CP001	5.87	5.40	4.66	4.37	–	4.53	4.26	–	3.41
CP002	4.57	4.24	3.24	2.98	–	3.04	2.80	–	2.32
CP003	2.37	2.22	1.71	1.61	–	1.63	1.53	–	1.25
CP004	2.43	2.36	1.88	1.79	–	1.80	1.71	–	1.40
CP005	2.97	2.74	2.18	2.01	–	2.05	1.89	–	1.57
CP006	3.60	3.28	2.46	2.27	–	2.28	2.07	–	1.77
CP007	2.93	2.62	2.13	1.97	–	2.03	1.88	–	1.53

Table 9 (continued)

Outcrop	1/3	1/5	3/3A	3/5A	3/10A	3/3G	3/5G	3/10G	50%
CP010	5.17	4.66	3.50	3.33	–	3.35	3.15	–	2.59
CP012	3.87	3.38	2.62	2.50	–	2.47	2.38	–	1.95
CP013	3.67	3.36	2.58	2.38	–	2.39	2.23	–	1.86
CP014	2.47	2.30	1.94	1.80	–	1.91	1.76	–	1.40
CP015	3.67	3.34	2.50	2.31	2.11	2.32	2.16	–	1.80
CP017	7.37	6.18	5.76	4.93	4.02	5.62	4.80	3.92	3.85
CP018	0.83	0.72	0.57	0.51	–	0.53	0.47	–	0.40
CP019	1.40	1.20	1.01	0.89	–	0.95	0.84	–	0.69
CP020	1.97	1.90	1.50	1.42	–	1.39	1.33	–	1.11
CP021	9.13	8.30	6.23	5.98	–	6.06	5.73	–	4.66
CP022	5.60	5.16	4.53	4.04	3.46	4.40	3.90	3.34	3.15
CP023	5.67	5.20	4.12	3.78	3.26	3.89	3.59	3.12	2.95
CP024	3.50	3.18	2.54	2.42	2.10	2.34	2.28	1.97	1.89
CP026	21.33	20.20	16.56	15.87	13.65	16.15	15.46	13.24	12.38
CP027	2.73	2.54	2.18	1.96	1.67	2.12	1.90	1.61	1.53
CP030	2.23	2.08	1.66	1.54	1.38	1.58	1.47	1.30	1.20
CP031	2.17	2.10	1.64	1.61	1.47	1.61	1.54	1.42	1.26
CP033	5.37	4.94	3.87	3.71	3.24	3.74	3.58	3.13	2.89

Appendix 3

Table 10 Summary of column heights and mass eruption rates for Layer 3. MER was derived using Wilson and Walker (1987)

	1/3	1/5	3/3A	3/5A	3/3G	3/5G	50th percentile	Av. AT1	Av. AT2
Column height (km)									
C&S (1986)—0.8	–	–	25.1	–	25.6	22.7	22.0	23.9	24.5
C&S (1986)—1.6	27.3	25.8	25.6	24.6	25.6	22.9	22.9	25.0	25.3
C&S (1986)—3.2	25.4	21.5	21.0	20.8	19.6	20.3	19.0	21.1	21.4
C&S (1986)—6.4	20.3	18.6	–	–	–	–	–	19.5	19.5
C&S (1986)—0.8–1.6 only	27.3	25.8	25.4	24.6	25.6	22.8	22.5	24.8	25.2
C&S (1986)—All isopleth lines	24.3	22.0	23.9	22.7	23.6	22.0	21.3	22.8	23.1
Pyle (1989)	29.6	29.0	26.7	26.1	26.1	24.6	–	27.0	27.0
Mass discharge rate ($\times 10^7$ kgs^{-1})									
C&S (1986)—0.8	–	–	5.2	–	5.7	3.5	3.1	4.4	4.8
C&S (1986)—1.6	7.3	5.9	5.7	4.8	5.7	3.6	3.6	5.2	5.5
C&S (1986)—3.2	5.5	2.8	2.6	2.5	1.9	2.2	1.7	2.8	2.9
C&S (1986)—6.4	2.2	1.6	–	–	–	–	–	1.9	1.9
C&S (1986)—0.8–1.6 only	7.3	5.9	5.5	4.8	5.7	3.6	3.4	5.2	5.5
C&S (1986)—All isopleth lines	4.6	3.1	4.3	3.5	4.1	3.1	2.7	3.6	3.8
Pyle (1989)	10.0	9.3	6.7	6.1	6.1	4.8	–	7.2	7.2

Av. AT1 Average over all averaging techniques, *Av. AT2* Average over all averaging techniques, except 50th percentile, *C&S (1986)* Carey and Sparks (1986)

Appendix 4

Table 11 Summary of column heights and mass eruption rates for Layer 5. MER was derived using Wilson and Walker (1987)

	1/3	1/5	3/3A	3/5A	3/10A	3/3G	3/5G	3/10G	50th percentile	Av. AT1	Av. AT2	Av. AT3
Column height (km)												
C&S (1986)—0.8	–	–	25.5	24.7	–	25	25	–	–	25.1	25.1	25.1
C&S (1986)—1.6	28	26.7	25.7	25	22.9	25.8	25.2	23	21.2	24.8	25.3	26.1
C&S (1986)—3.2	28	25.8	22.3	25.5	20	23.7	–	–	17.6	23.3	24.2	25.1
C&S (1986)—6.4	24.6	25.3	24.3	–	–	–	–	–	–	24.7	24.7	24.7
C&S (1986)—0.8–1.6 only	28.0	26.7	25.6	24.9	22.9	25.4	25.1	23.0	21.2	24.8	25.2	25.9
C&S (1986)—All isopleth lines	26.9	25.9	24.5	25.1	21.5	24.8	25.1	23.0	19.4	24.0	24.6	25.4
Pyle (1989)	28.7	28.7	25.1	24.6	–	26.6	26.6	–	–	26.7	26.7	26.7
Mass discharge rate ($\times 10^7$ kgs^{-1})												
C&S (1986)—0.8	–	–	5.6	4.9	–	5.2	5.2	–	–	5.2	5.2	5.2
C&S (1986)—1.6	8.1	6.7	5.8	5.2	3.6	5.9	5.3	3.7	2.7	5.2	5.5	6.2
C&S (1986)—3.2	8.1	5.9	3.3	5.6	2.1	4.2	–	–	1.3	4.3	4.8	5.4
C&S (1986)—6.4	4.8	5.4	4.6	–	–	–	–	–	–	4.9	4.9	4.9
C&S (1986)—0.8–1.6 only	8.1	6.7	5.7	5.0	3.6	5.5	5.2	3.7	2.7	5.1	5.4	6.0
C&S (1986)—All isopleth lines	6.9	6.0	4.7	5.2	2.8	5.0	5.2	3.7	1.9	4.6	4.9	5.5
Pyle (1989)	9.0	9.0	5.2	4.8	–	6.6	6.6	–	–	6.9	6.9	6.9

Av. AT1 Average over all averaging techniques, *Av. AT2* Average over all averaging techniques, except 50th percentile, *Av. AT3* Average over all averaging techniques, except 50th percentile and 10-clast, *C&S (1986)* Carey and Sparks (1986)

References

Ablay GJ, Ernst GGJ, Marti J, Sparks RSJ (1995) The 2 ka subplinian eruption of Montaña Blanca, Tenerife. Bull Volcanol 57(5):337–355

Adams NK, de Silva SL, Self S, Salas G (2001) The physical volcanology of the 1600 eruption of Huaynaputina, southern Peru. Bull Volcanol 62(8):493–518

Andronico D, Cioni R (2002) Contrasting styles of Mount Vesuvius activity in the period between the Avellino and Pompeii Plinian eruptions, and some implications for assessment of future hazards. Bull Volcanol 64(6):372–391

Barberi F, Coltelli M, Frullani A, Rosi M (1995) Chronology and dispersal characteristics of recently (last 5000 years) erupted tephra of Cotopaxi (Ecuador): implications for long-term eruptive forecasting. J Volcanol Geotherm Res 69(3–4):217–239

Bonadonna C, Costa A (2010) Modeling of tephra sedimentation from volcanic plumes. In: Fagents SA, Gregg TKP, Lopes RMC (eds) Modeling volcanic processes: the physics and mathematics of volcanism. Cambridge University Press, Cambridge

Bonadonna C, Houghton B (2005) Total grain-size distribution and volume of tephra-fall deposits. Bull Volcanol 67(5):441–456

Bonadonna C, Ernst GG, Sparks RSJ (1998) Thickness variations and volume estimates of tephra fall deposits; the importance of particle Reynolds number. J Volcanol Geotherm Res 81:173–187

Bryan SE, Cas RAF, Martí J (2000) The 0.57 Ma plinian eruption of the Granadilla Member, Tenerife (Canary Islands): an example of complexity in eruption dynamics and evolution. J Volcanol Geotherm Res 103(1–4):209–238

Carey S, Sigurdsson H (1986) The 1982 eruptions of El Chichon volcano, Mexico (2): observations and numerical modelling of tephra-fall distribution. Bull Volcanol 48(2–3):127–141

Carey S, Sigurdsson H (1987) Temporal variations in column height and magma discharge rate during the 79 A.D. eruption of Vesuvius. Geol Soc Am Bull 99(2):303–314

Carey S, Sparks RSJ (1986) Quantitative models of the fallout and dispersal of tephra from volcanic eruption columns. Bull Volcanol 48(2–3):109–125

Carey S, Sigurdsson H, Gardner J (1990) Variations in column height and magma discharge during the May 18, 1980 eruption of Mount St. Helens. J Volcanol Geotherm Res 43(1–4):99–112

Cioni R, Sulpizio R, Garruccio N (2003) Variability of the eruption dynamics during a Subplinian event: the Greenish Pumice eruption of Somma–Vesuvius (Italy). J Volcanol Geotherm Res 124(1–2):89–114

Cole PD, Queiroz G, Wallenstein N, Gaspar JL, Duncan A, Guest J (1995) An historic subplinian/phreatomagmatic eruption: the 1630 AD eruption of Furnas volcano, São Miguel, Azores. J Volcanol Geotherm Res 69(1–2):117–135

Connor LJ, Connor CB (2006) Inversion is the key to dispersion: understanding eruption dynamics by inverting tephra fallout. In: Mader HM, Connor CB, Coles SG, Connor LJ (eds) Statistics in volcanology special publications of IAVCEI, 1. Geological Society, London, pp 231–242

Costantini L, Bonadonna C, Houghton BF, Wehrmann H (2009) New physical characterization of the Fontana Lapilli basaltic Plinian eruption, Nicaragua. Bull Volcanol 71(3):337–355

Fierstein J, Hildreth W (1992) The plinian eruptions of 1912 at Novarupta, Katmai National Park, Alaska. Bull Volcanol 54 (8):646–684

Fierstein J, Nathenson M (1992) Another look at the calculation of fallout tephra volumes. Bull Volcanol 54(2):156–167

Gardner J, Tait S (2000) The caldera-forming eruption of Volcan Ceboruco, Mexico. Bull Volcanol 62(1):20–33

Giannetti B (1996) Volcanology of trachytic and associated basaltic pyroclastic deposits at Roccamonfina volcano, Roman Region, Italy. J Volcanol Geotherm Res 71(2–4):229–248

Giannetti B, De Casa G (2000) Stratigraphy, chronology, and sedimentology of ignimbrites from the White Trachytic Tuff, Roccamonfina Volcano, Italy. J Volcanol Geotherm Res 96(3–4):243–295

Hall M, Mothes P (2008) The rhyolitic–andesitic eruptive history of Cotopaxi volcano, Ecuador. Bull Volcanol 70(6):675–702

Hildreth W, Drake RE (1992) Volcán Quizapu, Chilean Andes. Bull Volcanol 54(2):93–125

Jurado-Chichay Z, Walker GPL (2001) The intensity and magnitude of the Mangaone subgroup plinian eruptions from Okataina Volcanic Centre, New Zealand. J Volcanol Geotherm Res 111(1–4):219–237

Kanisawa S, Yoshida T (1989) Genesis of the extremely low-K tonalites from the island arc volcanism. Bull Volcanol 51(5):346–354

Legros F (2000) Minimum volume of a tephra fallout deposit estimated from a single isopach. J Volcanol Geotherm Res 96(1–2):25–32

Limburg EM, Varekamp JC (1991) Young pumice deposits on Nisyros, Greece. Bull Volcanol 54(1):68–77

Lirer L, Pescatore T, Booth B, Walker GPL (1973) Two plinian pumice-fall deposits from Somma-Vesuvius, Italy. Geol Soc Am Bull 84(3):759–772

Luhr JF (2000) The geology and petrology of Volcán San Juan (Nayarit, México) and the compositionally zoned Tepic Pumice. J Volcanol Geotherm Res 95(1–2):109–158

McPhie J, Walker GPL, Christiansen RL (1990) Phreatomagmatic and phreatic fall and surge deposits from explosions at Kilauea volcano, Hawaii, 1790 a.d.: Keanakakoi Ash Member. Bull Volcanol 52(5):334–354

Milner D, Cole JW, Wood CP (2003) Mamaku Ignimbrite: a caldera-forming ignimbrite erupted from a compositionally zoned magma chamber in Taupo Volcanic Zone, New Zealand. J Volcanol Geotherm Res 122(3–4):243–264

Naranjo JA, Stern CR (1998) Holocene explosive activity of Hudson Volcano, southern Andes. Bull Volcanol 59(4):291–306

Newhall CG, Self S (1982) The volcanic explosivity index/VEI/-An estimate of explosive magnitude for historical volcanism. J Geophys Res 87:1231–1238

Palladino DM, Agosta E (1997) Pumice fall deposits of the western Vulsini Volcanoes (central Italy). J Volcanol Geotherm Res 78(1–2):77–102

Papale P, Rosi M (1993) A case of no-wind plinian fallout at Pululagua caldera (Ecuador): implications for models of clast dispersal. Bull Volcanol 55(7):523–535

Pérez W, Alvarado GE, Gans PB (2006) The 322 ka Tiribí Tuff: stratigraphy, geochronology and mechanisms of deposition of the largest and most recent ignimbrite in the Valle Central, Costa Rica. Bull Volcanol 69(1):25–40

Pyle DM (1989) The thickness, volume and grainsize of tephra fall deposits. Bull Volcanol 51(1):1–15

Pyle DM (1995) Mass and energy budgets of explosive volcanic eruptions. Geophys Res Lett 5:563–566

Pyle DM (2000) Sizes of volcanic eruptions. In: Sigurdsson H, Houghton BF, McNutt S, Rymer H, Stix J (eds) Encyclopedia of volcanoes. Academic Press, San Diego, pp 263–269

Rodríguez SR, Siebe C, Komorowski JC, Abrams M (2002) The Quetzalapa Pumice: a voluminous late Pleistocene rhyolite deposit in the eastern Trans-Mexican Volcanic Belt. J Volcanol Geotherm Res 113(1–2):177–212

Rolandi G, Petrosino P, Mc Geehin J (1998) The interplinian activity at Somma–Vesuvius in the last 3500 years. J Volcanol Geotherm Res 82(1–4):19–52

Rolandi G, Munno R, Postiglione I (2004) The AD 472 eruption of the Somma volcano. J Volcanol Geotherm Res 129(4):291–319

Rosi M (1998) Plinian eruption columns: particle transport and fallout. In: Freundt A, Rosi M (eds) From magma to tephra. Elsevier, Amsterdam, pp 139–172

Rosi M, Principe C, Vecci R (1993) The 1631 Vesuvius eruption. A reconstruction based on historical and stratigraphical data. J Volcanol Geotherm Res 58(1–4):151–182

Rosi M, Vezzoli L, Castelmenzano A, Grieco G (1999) Plinian pumice fall deposit of the Campanian Ignimbrite eruption (Phlegraean Fields, Italy). J Volcanol Geotherm Res 91(2–4):179–198

Rossotti A, Carrasco-Núñez G, Rosi M, Di Muro A (2006) Eruptive dynamics of the "Citlaltépetl Pumice" at Citlaltépetl volcano, Eastern Mexico. J Volcanol Geotherm Res 158(3–4):401–429

Scasso RA, Corbella H, Tiberi P (1994) Sedimentological analysis of the tephra from the 12–15 August 1991 eruption of Hudson volcano. Bull Volcanol 56(2):121–132

Self S (1976) The recent volcanology of Terceira, Azores. J Volcanol Geotherm Res 132(6):645–666

Sigurdsson H, Carey S (1989) Plinian and co-ignimbrite tephra fall from the 1815 eruption of Tambora volcano. Bull Volcanol 51(4):243–270

Sigurdsson H, Cashdollar S, Sparks SRJ (1982) The eruption of Vesuvius in A. D. 79: reconstruction from historical and volcanological evidence. Am J Archaeol 86(1):39–51

Sottili G, Palladino DM, Zanon V (2004) Plinian activity during the early eruptive history of the Sabatini Volcanic District, Central Italy. J Volcanol Geotherm Res 135(4):361–379

Sparks RSJ (1986) The dimensions and dynamics of volcanic eruption columns. Bull Volcanol 48(1):3–15

Sparks RSJ, Wilson L, Sigurdsson H (1981) The pyroclastic deposits of the 1875 eruption of Askja, Iceland. Philos Trans R Soc Lond 299(1447):241–273

Sulpizio R (2005) Three empirical methods for the calculation of distal volume of tephra-fall deposits. J Volcanol Geotherm Res 145:315–336

Suzuki T, Katsui Y, Nakamura T (1973) Size distribution of the Tarumai Ta-b pumice-fall deposit. Bull Volcanol Soc Japan 18:47–63

Thórarinsson S (1954) The tephra fall from Hekla on March 29th 1947. The eruption of Hekla 1947–1948. Soc Sci Islandica 2(3):68

Thouret JC, Juvigne E, Gourgaud A, Boivin P (2002) Reconstruction of the AD 1600 Huaynaputina eruption based on the correlation of geologic evidence with early Spanish chronicles. J Volcanol Geotherm Res 115(3–4):529–570

Volentik A, Bonadonna C, Connor CB, Connor LJ, Rosi M (2010) Modeling tephra dispersal in absence of wind: insights from the climactic phase of the 2450 BP Plinian eruption of Pululagua volcano (Ecuador). J Volcanol Geotherm Res 193(1–2):117–136

Walker GPL (1971) Grainsize characteristics of pyroclastic deposits. J Geol 79:696–714

Walker GPL (1980) The Taupo pumice: product of the most powerful known (ultraplinian) eruption. J Volcanol Geotherm Res 8(1):69–94

Walker GPL (1981) The Waimihia and Hatepe plinian deposits from the rhyolitic Taupo Volcanic Centre. NZ J Geol Geophys 24:305–325

Walker GPL, Croasdale R (1971) Two plinian-type eruptions in the Azores. J Geol Soc London 127:17–55

Walker GPL, Self S, Wilson L (1984) Tarawera 1886, New Zealand—a basaltic plinian fissure eruption. J Volcanol Geotherm Res 21 (1–2):61–78

Wehrmann H, Bonadonna C, Freundt A, Houghton BF, Kutterolf S (2006) Fontana Tephra: a basaltic Plinian eruption in Nicaragua. Geol Soc Am Spec Pap 412:209–223

Williams SN, Self S (1983) The October 1902 plinian eruption of Santa Maria volcano, Guatemala. J Volcanol Geotherm Res 16(1–2):33–56

Wilson CJN (1993) Stratigraphy, chronology, styles and dynamics of late quaternary eruptions from Taupo Volcano, New Zealand. Philos Trans R Soc Lond 343(1668):205–306

Wilson L, Walker GPL (1987) Explosive volcanic eruptions—VI. Ejecta dispersal in plinian eruptions: the control of eruption conditions and atmospheric properties. Geophys J R Astr Soc 89(2):657–679